Journal of Crystal Growth 89 (1988) 301–307
North-Holland, Amsterdam

PHASE RELATION AND THE EFFECTS OF ORDERING IN $(AgCd_2In)_p(CuIn)_{2y}Mn_{4z}Te_4$ ($p+y+z=1$) ALLOYS

Miguel QUINTERO, Pedro GRIMA, Eunice GUERRERO, Rafael TOVAR and John C. WOOLLEY *

Laboratoria de Cristales, Centro de Estudios de Semiconductores, Facultas de Ciencias, Departamento de Fisica, Universidad de Los Andes, Mérida, Venezuela

Received 21 January 1988

The T versus composition phase diagram of the alloy system $(AgCd_2In)_p(CuIn)_{2y}Mn_{4z}Te_4$ was investigated in the range $0 < z < 0.7$ by differential thermal analysis (DTA) and X-ray diffraction measurements. Samples were prepared for various lines of constant p/y ratio and the $T(z)$ diagram determined for each line. Values of lattice parameters were determined for all samples and the limits of single-phase solid solution estimated. In addition to liquidus and solidus curves, the zincblende–chalcopyrite and Mn-disordered–Mn-ordered transition lines were determined, since these phase fields are the ones of interest in measurements of energy gap and magnetic properties.

1. Introduction

In recent work [1–3], a new series of semimagnetic semiconductor alloys (SMSA) based on the I–III–VI_2 compounds have been investigated. In combination with MnTe, in order to retain semiconductor behaviour, it is necessary to preserve the electron-to-atom ratio by replacing the pair (I–III) by 2 Mn so that a series of alloys of the form $(I\text{–}III)_{1-z}Mn_{2z}Te_2$ have been produced and studied. In most cases the range of solid solution in the adamantine structure exceeds $z = 0.25$ and is as large as 0.72 for the case of $(AgIn)_{1-z}Mn_{2z}Te_2$ [2]. The composition range of these materials can be extended by including II–VI compounds as a further component. Thus the alloys $Cd_{2x}(CuIn)_yMn_{2z}Te_2$ and $Cd_{2x}(AgIn)_yMn_{2z}Te_2$ ($x+y+z=1$) have been investigated in some detail [1,2] with ranges of solid solution, lattice parameter and optical values being determined. Aresti et al. [3] have reported the $T(z)$ diagram of the $(CuIn)_{1-z}Mn_{2z}Te_2$ alloys, and in more recent work [4,5] the $T(z)$ diagrams of $(CuIn)_{1-z}Mn_{2z}Te_2$, $(AgIn)_{1-z}Mn_{2z}Te_2$ and $(AgGa)_{1-z}Mn_{2z}Te_2$ have been investigated. Woolley et al. [6] have studied the relation between the crystallography, optical properties and magnetic properties of the $(I\text{–}III)_{1-z}Mn_{2z}Te_2$ (I: Cu, Ag; III: In, Ga) alloy systems. Here, the study of the chalcopyrite alloys has been extended to other sections of the general system $Cd_{2w}(AgIn)_x(CuIn)_yMn_{2z}Te_2$ ($w+x+y+z=1$).

In the semimagnetic semiconductors based on II–VI compounds, e.g. $Cd_{1-z}Mn_zTe$, the Mn atoms are distributed at random on the cation sublattice, this being an essential requirement for the occurrence of spin-glass behaviour observed at low temperatures. However, in the case of the I–III–VI_2 derived SMSA, X-ray, optical energy gap and magnetic susceptibility measurements [1,2,6] have shown that while the alloys can be produced with this random Mn configuration, the equilibrium condition at lower temperatures has the Mn atoms crystallographically ordered (or partially ordered) on the cation sublattice. The details of this crystallographically ordered structure are still being investigated. This Mn ordering has a very pronounced effect on the magnetic properties, so that the magnetic behaviour of Mn-ordered and Mn-disordered alloys of the same composition are very different [6].

* Permanent address: Physics Department, University of Ottawa, Ottawa, Ontario, Canada K1N 6N5.

In order to investigate both the crystallographic effects and the differences in magnetic phenomena, it is necessary to choose the heat treatment of the alloys so as to produce the required Mn-ordered or Mn-disordered conditions. For this purpose a detailed knowledge of the T versus composition phase diagram is required. Recently, the $T(z)$ diagrams of $(CuIn)_{1-z}Mn_{2z}Te_2$, $(AgIn)_{1-z}Mn_{2z}Te_2$ and $(AgGa)_{1-z}Mn_{2z}Te_2$ have been determined [3–5] and in more recent work, $T(z)$ diagrams for sections of the $Cd_{2x}(AgIn)_y Mn_{2z}Te_2$ system have been investigated [7]. In the present work, this investigation has been extended to the study of the $T(z)$ diagrams of various sections of the general system.

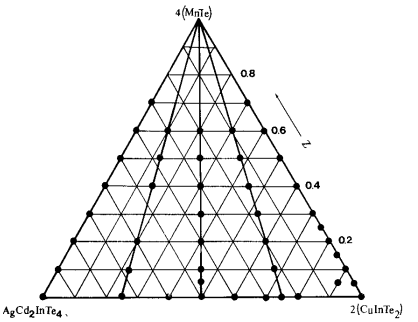

Fig. 2. Equilateral triangle showing compositions investigated in this work.

2. Materials to be investigated

The system $Cd_{2w}(AgIn)_x(CuIn)_yMn_{2z}Te_2$ can be conveniently represented by a regular tetrahedron as shown in fig. 1 with 2(CdTe), $AgInTe_2$, $CuInTe_2$ and 2(MnTe) at the four apices. The systems $Cd_{2w}(CuIn)_yMn_{2z}Te_2$ [1], $Cd_{2w}(AgIn)_x Mn_{2z}Te_2$ [2] and $Cd_{2w}(AgIn)_x(CuIn)_yTe_2$ [8] already reported form three faces of the tetrahedron. The other face, $(AgIn)_x(CuIn)_yMn_{2z}Te_2$ is still being studied. In the present work, the section given by $x = w(=p/2)$ is being studied. This section has the form $Cd_p(AgIn)_{p/2}(CuIn)_y Mn_{2z}Te_2$ which can be more conveniently written as $(AgCd_2In)_p(CuIn)_{2y}Mn_{4z}Te_4$. The section is an isoceles triangle in fig. 1 but can conveniently be represented by the usual equilateral triangle with coordinates p, y and z as shown in fig. 2.

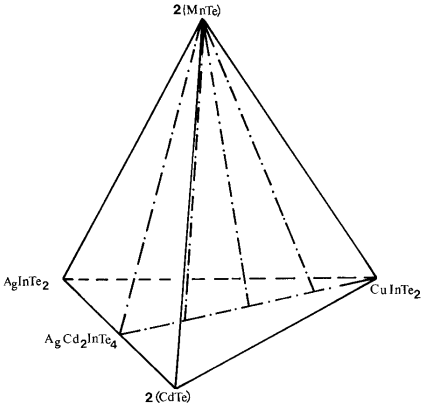

Fig. 1. General diagram showing the section investigated in the present work. Lines in this section with $y = 0$, $p = 3y$, $p = y$, $z = 0$ and $y = 3p$ are shown dash-dotted.

In order to produce useful $T(z)$ diagrams, samples were prepared for the sections given by $p = 3y$, $p = y$, $3p = y$, $p = 0$ and $y = 0$. Also, since the interest of the programme is in semimagnetic semiconductors, values of z up to an upper limit of 0.7 only were used, and the MnTe rich phases were not investigated.

3. Preparation of alloys and DTA measurements

All of the alloys used were produced by the usual melt and anneal technique [9]. The components of each 1.5 g sample were sealed under vacuum in a quartz capsule, which had previously been coated with carbon in order to prevent reaction of the alloys with the quartz. The components were then melted together at 1150 °C and annealed to equilibrium. As in all such multicomponent alloys, the appropriate temperature of anneal is not easily determined until the T versus com-

position phase diagram is known for each section. However, the results for the sections $(CuIn)_{1-z}Mn_{2z}Te_2$ and $(AgIn)_{1-z}Mn_{2z}Te_2$ [1,2,4] already investigated show that an annealing temperature of 600 °C should be satisfactory and this value was used here. It is found that equilibrium at fairly low temperature is needed if peaks corresponding to order–disorder and chalcopyrite–zincblende transitions are to be observed in the heating DTA runs. It has been found that at least 20–30 days of annealing are necessary to obtain equilibrium conditions at 600 °C, since long range diffusion may be required after the initial cooling from the melt. However, once this has been achieved, the zincblende–chalcopyrite and order–disorder transitions, which occur below 600 °C in these systems and which involve only short range diffusion, can occur in much shorter times.

Guinier X-ray powder photographs were used to check the conditions of the annealed samples and to determine the phases which were present. Values of lattice parameter were determined for the zincblende and chalcopyrite phases, these results having been reported previously [10].

Transition temperatures were obtained from DTA measurements [11], with silver or gold used as the reference material. The charge was of powdered alloy of approximately 100 mg weight. The temperatures of the sample and the reference were measured with chromel–alumel thermocouples, the difference signal between sample and reference and also the temperature signal being registered on a two-pen chart recorder. Each phase transition temperature was determined from the base line intercept of the tangent to the leading edge of the peak in the difference signal. Both heating and cooling runs were made for each sample.

4. Results and discussion

The $T(z)$ diagram for the $(CuIn)_{1-z}Mn_{2z}Te_2$ section (i.e. $p = 0$) has been given previously [3,4], and recently T versus composition diagrams have been obtained for the $Cd_{2x}(AgIn)_yMn_{2z}Te_2$ alloys [7] and the $x = y$ section in that case is the

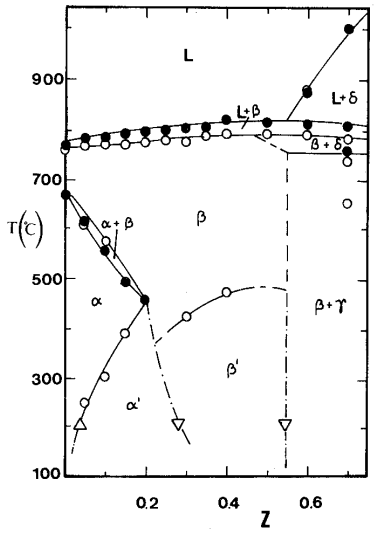

Fig. 3. $T(z)$ diagram for the $(CuIn)_{1-z}Mn_{2z}Te_2$ section (i.e. $p = 0$). α is the Mn-disordered chalcopyrite, α' the Mn-ordered chalcopyrite, β the Mn-disordered zincblende, β' the Mn-ordered zincblende, and δ and γ are the NaCl and NiAs structures of MnTe, respectively. (▽) Data from X-ray; (△) data from E_0; (○) heating run; (●) cooling run.

$y = 0$ section of the present system. In addition, the $z = 0$ section of the present work is the $y = z$ section of the system $(CuIn)_x(AgIn)_yCd_{2z}Te_2$, the data for which will be published elsewhere [12]. For comparison purposes, these three diagrams are shown in figs. 3, 4 and 5. The $T(z)$ diagrams for the sections $p = 3y$, $p = y$ and $3p = y$ are shown in figs. 6, 7 and 8 respectively. In these diagrams, boundaries determined directly from DTA measurements are shown as solid lines. However, some boundaries cannot be determined from the DTA data and these need to be estimated from the lattice parameter and energy gap values determined previously [10]. These boundaries are shown as dash-dotted lines in the $T(z)$ diagrams. Finally, dashed lines have been used to indicate lines which are estimated only.

As has been shown previously [13], $CuInTe_2$ has the chalcopyrite structure α up to 670 °C and then becomes zincblende β up to 770 °C where it becomes liquid. However, $AgInTe_2$ is α chal-

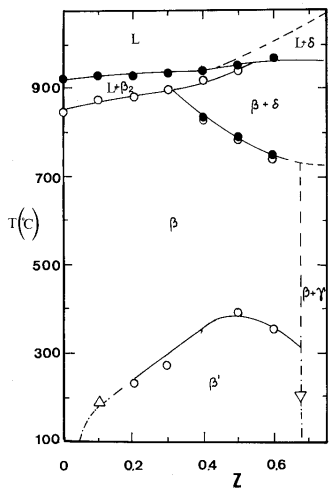

Fig. 4. $T(z)$ diagram for the $(AgCd_2In)_{1-z}Mn_{4z}Te_4$ section (i.e. $y = 0$). β is the Mn-disordered zincblende, β' the Mn-ordered zincblende, and δ and γ are the NaCl and NiAs structures of MnTe, respectively. (▽) Data from X-ray; (△) data from E_0; (○) heating run; (●) cooling run.

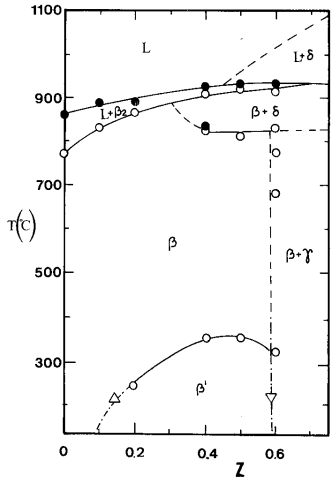

Fig. 6. $T(z)$ diagram for the $p = 3y$ line. β is the Mn-disordered zincblende, β' the Mn-ordered zincblende, and δ and γ are the NaCl and NiAs structures of MnTe, respectively. (▽) Data from X-ray; (△) data from E_0; (○) heating run; (●) cooling run.

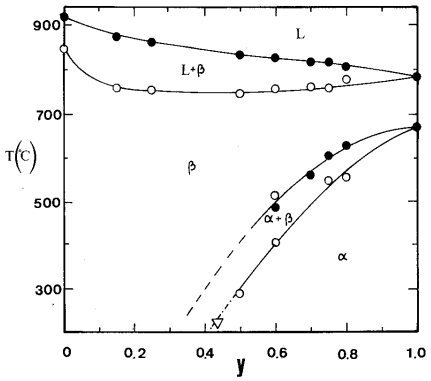

Fig. 5. $T(z)$ diagram for the $(AgCd_2In)_{1-y}(CuIn)_{2y}Te_4$ section (i.e. $z = 0$). α is the chalcopyrite and β the zincblende structure. (▽) Data from X-ray; (○) heating run; (●) cooling run.

copyrite to 630 °C, β zincblende to 660 °C, above which temperature it splits up into a $(L + \beta_2)$ two-phase form up to liquidus at 685 °C, the β and β_2 phases both being zincblende but of different composition.

The form of the bounding sections of the present alloys, i.e. $z = 0$ (fig. 5), $p = 0$ (fig. 3) and $y = 0$ (fig. 4) reflect this behaviour of the compounds. Considering the lower temperature range, i.e. mainly the single phase solid fields, it is seen that the $z = 0$ section shows complete solid solution in the β phase from 750 to 670 °C and below this, wide ranges of single phase α and β fields separated by a relatively narrow $(\alpha + \beta)$ two phase field. This $(\alpha + \beta)$ field is present at all temperatures below 670 °C. The $p = 0$ section also shows wide solid solution in the α and β phases, but as shown by the X-ray results [1,10] the ranges of solid solution in the β phase is limited to $z \sim 0.55$ and for z greater than this there is a two-solid phase field $(\beta + \gamma)$, where γ is the NiAs structure

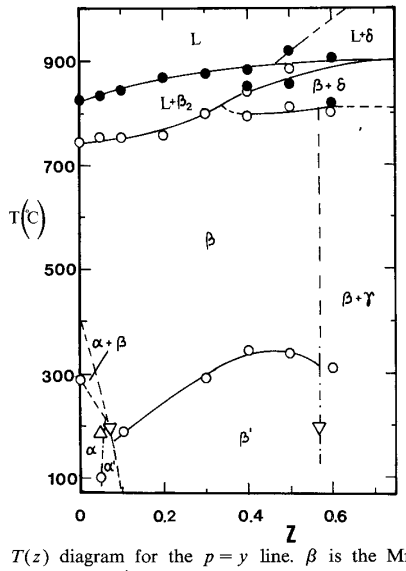

Fig. 7. $T(z)$ diagram for the $p = y$ line. β is the Mn-disordered zincblende, β' the Mn-ordered zincblende, and δ and γ are the NaCl and NiAs structures of MnTe, respectively. (▽) Data from X-ray; (△) data from E_0; (○) heating run; (●) cooling run.

of MnTe. The form of the $(\alpha + \beta)$ field in this section is different from that in the $z = 0$ section in that the $(\alpha + \beta)$ field is closed at $z \sim 0.2$ and for z greater than this the α–β boundary is a single line. This behaviour has been attributed [3] to a change from first order transition for $z < 0.2$ to second order transition for $z > 0.2$. It has been suggested [4] that the change in transition type is due to ordering of the Mn on the cation sublattice, and order–disorder boundaries (α–α' and β–β') are indicated in fig. 3. Thus the first order transition is associated with β–α interaction while the second order is associated with β–α' and β'–α'. The section $y = 0$ is different from the two described above in that no α field is present. The β field extends from $z = 0$ to $z \sim 0.68$ and above this value the two phase $(\beta + \gamma)$ field occurs. Again an order–disorder boundary β'–β is observed at lower temperatures.

The behaviour of the sections $p = 3y$, $p = y$ and $y = 3p$ in this lower temperature range is very similar to that of the bounding sections. The $p = 3y$ is very similar to that for $y = 0$, showing no α field and a wide range of β field limited to $z \sim 0.58$, above which value a two-phase $(\beta + \gamma)$ field occurs. Again an order–disorder transition (β'–β) is observed over most of the composition range for which the β phase occurs. The $p = y$ and $y = 3p$ sections show a gradual change to the form of the $p = 0$ section with a small α field for $p = y$ and a larger α field for the $y = 3p$ section, and the limit of the β field occurring at $z \sim 0.66$ for $p = y$ and $z \sim 0.58$ for $y = 3p$. In each case the $(\alpha + \beta)$ field is closed at some value of z due to ordering and order–disorder boundaries are indicated in both sections.

At temperatures above the limits of the β field, the diagrams are more complicated and the designation of the phases in the various fields has been guided by the work of Chiang et al. [14] and Aresti et al. [3]. Firstly, two different zincblende phases occur (14) accounting for the β_2 phase seen in the various sections. At the higher z values, two-phase fields involving a phase δ occur and

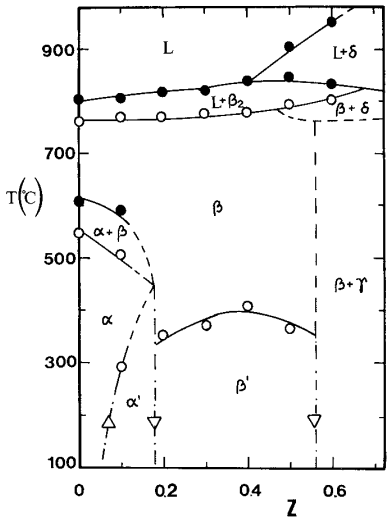

Fig. 8. $T(z)$ diagram for the $3p = y$ line. α is the Mn-disordered chalcopyrite, α' the Mn-ordered chalcopyrite, β the Mn-disordered zincblende, β' the Mn-ordered zincblende, and δ and γ are the NaCl and NiAs structures of MnTe, respectively. (▽) Data from X-ray; (△) data from E_0; (○) heating run; (●) cooling run.

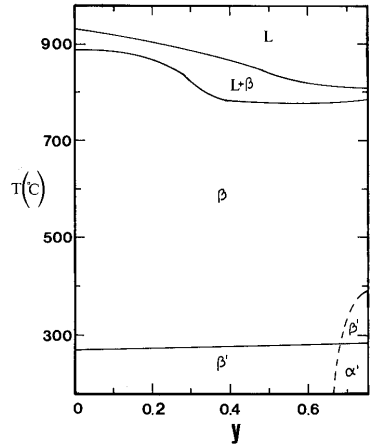

Fig. 9. $T(y)$ diagram for the $z = 0.25$ line, obtained by interpolation from the $T(z)$ data.

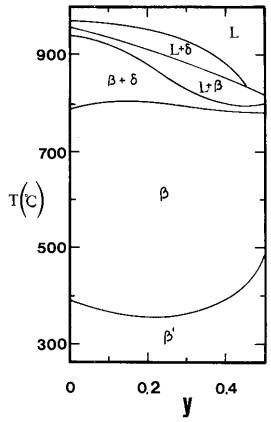

Fig. 10. $T(y)$ diagram for the $z = 0.50$ line, obtained by interpolation from the $T(z)$ data.

this has been identified [3] as the rocksalt structure shown by MnTe above 1050 °C but which exists at lower temperatures elsewhere in the general diagram. It is clear that, in general, none of the sections shown are pseudo-binary in character. However, for temperatures below 600 °C, these pseudo-binary conditions appear to be satisfied to a good approximation.

It is clear from the figures that because the α–α' and β–β' peaks are small and seen only with well-annealed samples on the initial heating runs, the transitions are not observed for all of the samples which should show them. However, one further factor can be used to indicate the positions of these boundaries. Figs. 3–8 show the variation of the transition temperatures with z for constant p/y ratio, but the values should also be consistent when plotted as a function of p or y at constant z, so that the temperature value for any given point should fit both $T(z)$ and $T(y)$ diagrams. As examples figs. 9 and 10 show $T(y)$ diagrams at constant z for $z = 0.25$ and $z = 0.5$.

As a final representation of the system, fig. 11 gives a perspective diagram showing the surfaces bounding the various single-phase solid fields. These fields are the ones of interest in the present work, and so the corresponding surfaces for two-phase fields, etc., have not been included. Lines have been included to show the boundaries in the sections with $y = 0$, $p = 3y$, $p = y$, $3p = y$ and $p = 0$ and also $z = 0.25$ and $z = 0.5$.

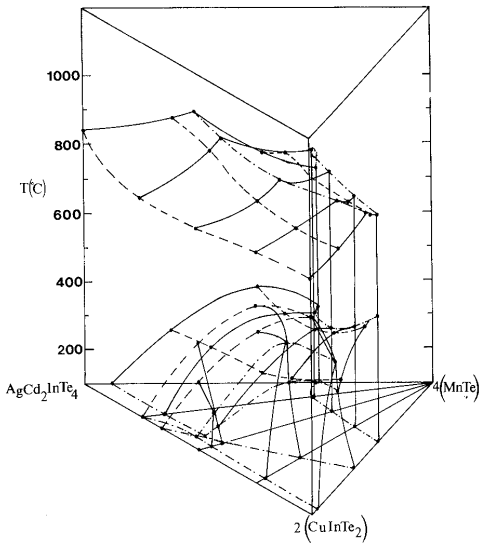

Fig. 11. Perspective diagram showing the surfaces bounding the various single-phase solid fields. Solid lines are lines in sections with p/y constant. Dashes lines are lines in sections with z constant. Dash-dotted lines are general lines. Points are positions where lines intersect.

5. Conclusions

The DTA and X-ray results for the $(AgCd_2In)_p(CuIn)_{2y}Mn_{4z}Te_4$ system show that a wide range of solid solutions occur for both the chalcopyrite and the zincblende structures and that for both structures an ordered form, attributed to the Mn ions ordering on the cation sublattice, occurs at approximately below 400 °C for values of $z > 0.05$.

The results show that the various sections cannot be treated as pseudo-binary, although for temperatures less than 600 °C this condition is satisfied to a good approximation.

Acknowledgements

The autors wish to thank G.S. Perez and F. Sanchez for technical assistance, and Margarita P. de Quintero for typing the manuscript. They are grateful to CDCHT (ULA) and CONICIT (Venezuela) for financial support.

References

[1] M. Quintero, L. Dierker and J.C. Woolley, J. Solid State Chem. 63 (1986) 110.
[2] M. Quintero and J.C. Woolley, Phys. Status Solidi (a) 92 (1985) 449.
[3] A. Aresti, L. Garbato, A. Geddo-Lehmann and P. Manca, in: Proc. 7th Intern. Conf. on Ternary and Multinary Compounds (Materials Research Society, Pittsburgh, PA, 1987) p. 497.
[4] M. Quintero, P. Grima, R. Tovar and J.C. Woolley, submitted.
[5] M. Quintero, R. Tovar, M. Al-Najjar, G. Lamarche and J.C. Woolley, submitted.
[6] J.C. Woolley, G. Lamarche, A. Manoogian, M. Quintero, L. Dierker, M. Al-Najjar, D. Proulx, C. Neal and R. Goudreault, in: Proc. 7th Intern. Conf. on Ternary and Multinary Compounds (Materials Research Society, Pittsburgh, PA, 1987) p. 479.
[7] M. Quintero, E. Guerrero, P. Grima and J.C. Woolley, submitted.
[8] E. Guerrero, M. Quintero and J.C. Woolley, submitted.
[9] R.G. Goodchild, U.H. Hughes, S.A. Lopez-Rivera and J.C. Woolley, Can. J. Phys. 60 (1982) 1096.
[10] M. Quintero, P. Grima, E. Guerrero, R. Tovar, G.S. Perez and J.C. Woolley, submitted.
[11] R. Chen and Y. Kirsh, The Analysis of Thermally Stimulated Processes, Intern. Series on the Science of the Solid State, Vol. 15 (Pergamon, Oxford, 1981) p. 97.
[12] E. Guerrero, M. Quintero and J.C. Woolley, submitted.
[13] L.S. Palatnik and E.I. Rogacheva, Soviet Phys.-Dokl. 12 (1967) 503.
[14] R.W. Chiang, D.F. O'Kane and D.R. Mason, J. Electrochem. Soc. 114 (1967) 759.